

# Quantum coherence and the invisible Universe: Subradiance as a dark matter mechanism

Martin Houde<sup>1\*</sup> and Fereshteh Rajabi<sup>2</sup>

<sup>1\*</sup>Department of Physics and Astronomy, The University of Western Ontario, 1151 Richmond Street, London, N6A 3K7, Ontario, Canada.

<sup>2</sup>Department of Physics and Astronomy, McMaster University, 1280 Main Street West, Hamilton, L8S 4L8, Ontario, Canada.

\*Corresponding author(s). E-mail(s): [mhoude2@uwo.ca](mailto:mhoude2@uwo.ca);  
Contributing authors: [rajabf1@mcmaster.ca](mailto:rajabf1@mcmaster.ca);

## Abstract

We investigate the role of quantum entanglement and coherence in suppressing radiation and explore its implications for dark matter. Using Dicke's framework, we demonstrate that entangled states in a gas at thermal equilibrium can lead to subradiance, trapping energy in dark quantum states and reducing radiation intensity. Applying this to the 21 cm line in dark matter halos, we find that quantum coherence renders the gas effectively dark. Moreover, entanglement results in a vanishing collision cross-section, consistent with the collisionless nature of dark matter observed in systems like the bullet cluster. We also show that absorption of incident radiation can exceed levels predicted by Beer's law, which holds only in the absence of coherence. These findings suggest that quantum entanglement and coherence may explain the non-luminous behavior of matter in dark matter halos, offering a novel perspective on dark matter and advancing the understanding of astrophysical radiative processes.

**Keywords:** entanglement, coherence, subradiance, dark matter

## 1 Introduction

It has been known since Dicke's original treatment of the spontaneous emission of coherent radiation [1] that the interaction between atoms composing a gas<sup>1</sup> through their common electromagnetic field leads to the formation of entangled quantum

---

<sup>1</sup>Although we focus on atoms in this paper, our analysis and discussions apply to molecular gases as well.

mechanical states, with significant implications for the spontaneous emission rates of photons emanating from the gas. As Dicke pointed out, atoms should not be considered as independent entities; instead, the entire gas must be treated as a single quantum mechanical system. While the material covered in his paper was broad, touching on several phenomena involving coherence and entanglement, much of the early work it inspired focused on superradiance.

Superradiance is a fundamental radiation process [2] in which the cooperative behavior of the atoms composing the gas leads to powerful bursts of coherent radiation. Indeed, superradiance can be thought of as “collective spontaneous emission,” where, instead of spontaneously emitting photons individually, the atoms cooperate in a coherent cascade of photon emission. Although the first experimental verification of superradiance occurred almost 20 years after Dicke’s work [3], astronomers remained largely unaware of this phenomenon and the intense research being conducted in the quantum optics community. This remained the case despite the earlier discovery of astronomical masers in the interstellar medium [4] and the complementarity between the maser action and superradiance [2, 5]. It is only recently that superradiance has been studied in an astronomical context and used to explain intense flares from maser-hosting regions in diverse environments [5–14]. Beyond improving our understanding and modeling of these systems, these studies have importantly established the presence of the type of coherence proposed by Dicke in astronomical media.

Dicke’s 1954 paper [1] also explicitly discussed another coherent radiation process, which later became known as subradiance. In contrast to superradiance, subradiance describes the suppression of photon emission compared to the typical spontaneous emission process. Dicke analyzed the trapping of energy in slow and dark quantum states and its consequences for the radiation intensity emanating from a gas. Subradiance was experimentally verified later than superradiance [15] and has only recently been observed in large clouds of cold atoms [16]. The latter experimental result is particularly relevant to us as we explore the possible existence of subradiant systems in astrophysical contexts.

More specifically, we ask the following question: Given that superradiance is known to occur in diverse astronomical environments, should we not also expect subradiance to be realized? We aim to answer this by exploring a possible link between subradiance and the presence of dark matter in the universe – one of the deepest mysteries in astrophysics since its manifestation in galactic rotation curves was discovered [17].

## 2 Results

### 2.1 Entangled quantum states and coherent behavior

In this section we revisit parts of Dicke’s work and focus on the trapping of energy within an atomic ensemble. We first focus on a two-atom system at resonance with Atom 1 at  $-z_0/2$  and Atom 2 at  $z_0/2$  on the  $z$ -axis. Given that single-atom transitions take place between the lower  $|a\rangle$  and upper  $|b\rangle$  levels of energies  $-\hbar\omega_0/2$  and  $\hbar\omega_0/2$ , respectively, appropriate internal states for the two-atom problem consist of [1, 18]

(see Appendices A and D)

$$|1, 1\rangle = |bb\rangle \quad (1)$$

$$|1, 0\rangle_\theta = \frac{1}{\sqrt{2}} \left( e^{i\frac{1}{2}kz_0 \cos \theta} |ab\rangle + e^{-i\frac{1}{2}kz_0 \cos \theta} |ba\rangle \right) \quad (2)$$

$$|1, -1\rangle = |aa\rangle \quad (3)$$

$$|0, 0\rangle_\theta = \frac{1}{\sqrt{2}} \left( e^{i\frac{1}{2}kz_0 \cos \theta} |ab\rangle - e^{-i\frac{1}{2}kz_0 \cos \theta} |ba\rangle \right). \quad (4)$$

Following Dicke [1], the kets  $|r, m\rangle$  are defined with the ‘‘cooperative’’ number  $r$  and ‘‘inversion’’ number  $m$ , which are analogous to spin-1/2 quantum numbers, with  $r \geq 0$  and  $|m| \leq r$  ( $|r, m\rangle_\theta = |r, m\rangle$  when  $\cos \theta = 0$ ). Note that  $k = 2\pi/\lambda$  with  $\lambda$  the radiation wavelength.

Given equations (1)-(4) it is straightforward to calculate the spontaneous emission transition rates per unit solid angle between the different states

$$\frac{d\gamma_{1,1 \rightarrow 1,0_\theta}}{d\Omega} = 2 \frac{d\Gamma}{d\Omega} \quad (5)$$

$$\frac{d\gamma_{1,1 \rightarrow 0,0_\theta}}{d\Omega} = 0 \quad (6)$$

$$\frac{d\gamma_{1,0_\theta \rightarrow 1,-1}}{d\Omega'} = 2 \cos^2 \left[ \frac{1}{2}kz_0 (\cos \theta' - \cos \theta) \right] \frac{d\Gamma}{d\Omega'} \quad (7)$$

$$\frac{d\gamma_{0,0_\theta \rightarrow 1,-1}}{d\Omega'} = 2 \sin^2 \left[ \frac{1}{2}kz_0 (\cos \theta' - \cos \theta) \right] \frac{d\Gamma}{d\Omega'} \quad (8)$$

with  $d\Gamma/d\Omega$  the spontaneous emission rate per unit solid angle of a single independent atom, and  $\theta$  and  $\theta'$  denoting the orientations of the first and second emitted photons, respectively, relative to the  $z$ -axis.

The signatures of entanglement and coherence are displayed in equations (7)-(8). That is, the enhancement of the transitions rates by a factor of ‘2’ is due to the entangled nature of the states given in equations (2) and (4), while the disappearance of the argument in the cosine and sine functions (i.e., when  $\cos \theta' = \cos \theta$ ) stems from coherence between the two emitted photons. We therefore find the existence of an angular correlation between successively emitted photons. More precisely, if the system starts in the  $|1, 1\rangle$  state, then after the emission of the first photon it will for sure end up in the symmetric  $|1, 0\rangle_\theta$  intermediate state. From there, we see that the second photon has a higher probability of being emitted in a direction where  $\cos \theta' = \cos \theta$  to reach the  $|1, -1\rangle$  ground state [18].

We will soon be interested in situations where the system is in thermal equilibrium where all the states for a given  $m$  value are initially equally populated. We thus focus on the transition rates between the  $m = 0$  and  $m = -1$  states given in equations (7)-(8). We can obtain the radiation intensity by, among other things, integrating these transition rates over the solid angle. Setting  $\cos \theta = 0$ , for simplicity, and initial conditions where the states  $|1, 0\rangle_\theta$  and  $|0, 0\rangle_\theta$  have equal but uncorrelated probabilities

of occupation (of  $1/2$ ), we can study the intensity in two opposite limits (see Appendix A.1).

For the infinite size sample  $kz_0 \rightarrow \infty$  we find

$$I_\infty(t) = \hbar\omega_0\Gamma e^{-\Gamma t}, \quad (9)$$

which is exactly the intensity from a single independent atom, with  $\Gamma$  is the single-atom free-space spontaneous emission rate (see equation A10).

On the other hand, in the idealized small sample limit  $kz_0 = 0$  the intensity becomes

$$I_{ss}(t) = \frac{1}{2}\hbar\omega_0(2\Gamma)e^{-2\Gamma t}. \quad (10)$$

The two-atom system will, on average, emit a photon half of the time but at twice the single-atom rate.

Another way to look at this is by considering the energy trapping efficiency defined as

$$\begin{aligned} \eta &= 1 - \frac{\int_0^\infty I_{ss}(t) dt}{\int_0^\infty I_\infty(t) dt} \\ &= 0.5. \end{aligned} \quad (11)$$

Again, we find that half of the internal energy initially stored in the system remains within it in the steady-state.

The small sample behavior is readily understood from equations (7)-(8) since in this case coherence happens for all radiation modes, resulting in the doubling and cancellation of the corresponding transition rates. The latter implies that  $|0, 0\rangle_\theta$  is a *dark state* and that its initial occupation probability is preserved at all times. This is where energy trapping originates. On the other hand, the behavior for  $kz_0 \rightarrow \infty$  is a global characteristic in the sense that it can only be discerned in the solid-angle-integrated transition rate. Even at very large separations some radiation modes will be coherent, but when considering all modes the two atoms behave as if they were independent (see equation A8).

This last observation is important since external factors can sometimes render specific radiation modes dominant over the rest. For example, elongated (e.g., cylindrical) geometries are often considered in studies of superradiance since in such cases radiation along the symmetry axis is favored [5, 18–20]. Similarly, a gas in the interstellar medium initially hosting a population inversion will be more likely to radiate in a direction where velocity coherence is accentuated, leading to a transient superradiance response [5, 13].

We also note that *superabsorption*, i.e., the converse of superradiance, takes place when the two-atom system is initially in the  $|1, -1\rangle$  ground state. When subjected to an incident one-photon field the transition rates of equations (5)-(8) are reversed [21]. Here again, there is angular correlation, but this time between successively absorbed photons (see Appendix A.1).

The calculations can be extended to a larger number of atoms. The internal states for an arbitrary number of atoms  $n$  is shown in Figure 1 along with the expected

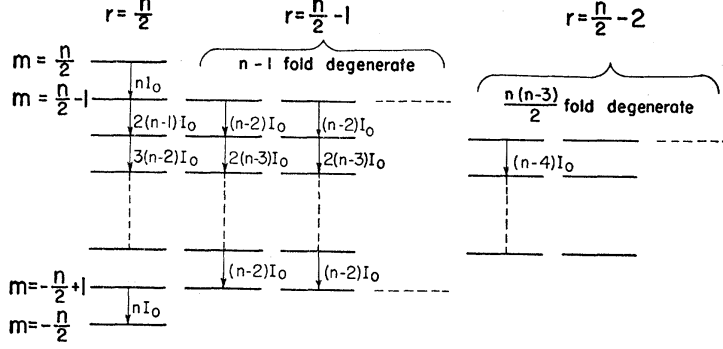


**Fig. 1** The coherent radiation rates between Dicke states in the small sample (i.e., when  $kz_0 \rightarrow 0$ ) or coherent limits. The number of atom contained in the radiating gas is  $n$ , while the states within the different coherent cascades are identified through the cooperative number  $0 \leq r \leq n/2$  and the inversion number  $-r \leq m \leq r$ . The radiative intensity (or rate) of a single atom is denoted by  $I_0$ . Taken from Dicke's original 1954 paper [1].

transition rates in the small sample (i.e.,  $kz_0 \rightarrow 0$ ) or coherent limits (taken from Dicke's original paper [1]). It is generally observed that, starting from a given  $m$  value, transitions are allowed only between states sharing the same cooperation number  $r$ , while rates systematically decrease as one moves rightward to lower  $r$  values.

It is shown in Appendix A.2 that for  $n \gg 1$  the energy trapping efficiency is  $\eta \approx 1 - \sqrt{2/n}$  when starting from  $m = 0$ . It is therefore clear that the combination of coherence and the entanglement of a large number of atoms can potentially lead to a significant amount of energy trapping within the gas. But one of our goals is to assess the level of energy trapping within the gas for finite and more realistic atomic separations in the interstellar medium. It is already obvious through our study of the two-atom system that the general case where  $kz_0 \neq 0$  will lead to a non-zero transition rate from the  $|0, 0\rangle_\theta$  'dark' state (see equations 4 and A8). This has for implication that all the energy initially stored in the system will eventually leak away. That is,  $\eta = 0$  in the steady-state and no energy trapping is realized in the long run.

## 2.2 Equilibrium conditions

To further our study of trapping and leaking of internal energy we move to the density matrix framework, using the master equation often used within the context of superradiance [20, 22] (see Appendix B).

For our two-atom problem the elements of the density matrix  $\hat{\rho}$  for the atomic system will be defined using the basis  $\{|1\rangle \equiv |1, 0\rangle, |2\rangle \equiv |0, 0\rangle, |3\rangle \equiv |1, -1\rangle\}$ , where  $|r, m\rangle$  is given in equations (1)-(3) with  $\cos\theta = 0$ . That is, we have  $\rho_{ij} = \langle i|\hat{\rho}|j\rangle$ . The solution of the master equation for the two-atom problem discussed in Sec. 2.1 is presented in Figure 2 for an atomic separation  $\Delta r = 0.02\lambda$  with the black curves tracing the time evolution of the corresponding populations. The initial conditions were set to  $\rho_{11}(0) = \rho_{22}(0) = 1/2$  and all other populations and coherences to zero. As can be inferred from the figure, no energy is trapped in the system as the  $\rho_{11}$  and  $\rho_{22}$  populations (corresponding to the  $|1, 0\rangle$  and  $|0, 0\rangle$  states, respectively) go to zero

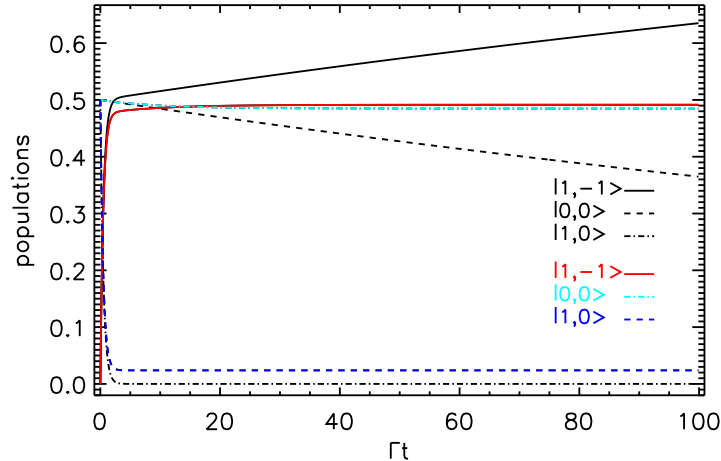


**Fig. 2** Solution of the two-atom system under the initial conditions  $\rho_{11}(0) = \rho_{22}(0) = 1/2$  and all other populations and coherences set to zero. The separation between the atoms was set to  $\Delta r = 0.02\lambda$ . The time evolution of the relevant populations are traced using the legend for the corresponding states. *Black curves*: no equilibrium conditions are enforced and the populations corresponding to  $m = 0$  will eventually all relax to zero. No energy trapping takes place in the steady-state (i.e., when  $\Gamma t \rightarrow \infty$ ). *Colored curves*: the equilibrium condition  $\rho_{11}^{\text{eq}} = \rho_{22}^{\text{eq}} = 1/2$  is applied with  $\Gamma T_1 = 10$ . Leakage is prevented and energy is trapped in the steady-state.

in the steady-state (i.e., as  $\Gamma t \rightarrow \infty$ ). The first (fast) state does so quickly (on a time-scale of  $\Gamma t \sim 1/2$ ) while the second (dark) state decays on a much longer time-scale, but will still eventually go down to zero.

The leakage of internal energy is stopped in the steady-state by enforcing equilibrium conditions for the populations. In Appendix B, we show how this happens through the introduction of a relaxation term acting on a time-scale  $T_1$  and a constant pump term, which we then define as  $\rho_{jj}^{\text{eq}}/T_1$ , with  $\rho_{jj}^{\text{eq}}$  the equilibrium condition for the corresponding population.

In Figure 2 we also show, using the colored curves and legend, the two-atom system response when  $\rho_{11}^{\text{eq}} = \rho_{22}^{\text{eq}} = 1/2$ ,  $\rho_{33}^{\text{eq}} = 0$  and  $\Gamma T_1 = 10$ . Since internal energy trapping is due to non-zero steady-state values in the upper populations  $\rho_{11}$  and  $\rho_{22}$ , we find that the presence of equilibrium conditions effectively causes this trapping to take place. More precisely, we find  $\approx 0.5$  of the total energy remaining in the two  $m = 0$  states for an energy trapping efficiency  $\eta \simeq 0.46$ .

Such analysis can be extended to cases involving a larger number of atoms. It will then generally be the case that the coherences  $\rho_{ij}$ , with  $i \neq j$ , will come into play. We therefore follow the usual practice of introducing a dephasing term scaling as  $-\rho_{ij}/T_2$ , with  $T_2$  the corresponding time-scale, to account for external factors acting to reduce coherence in the system.

Figure 3 shows the master equation solution for a system consisting of two two-atom pairs located a distance  $0.1\lambda$  apart; the two atoms forming one pair are still separated by  $\Delta r = 0.02\lambda$ . The solution is presented using the basis  $\{|aa\rangle|1,0\rangle, |aa\rangle|0,0\rangle, |1,0\rangle|aa\rangle, |0,0\rangle|aa\rangle, |aa\rangle|aa\rangle\}$  to ‘preserve’ the identity of the two pairs.

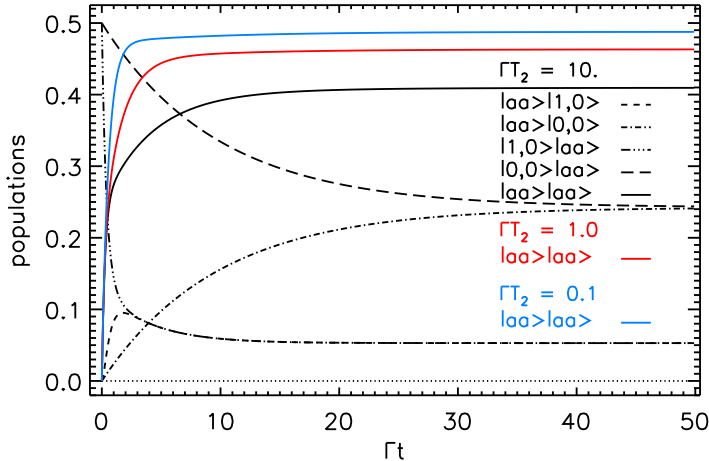


**Fig. 3** The master equation solution for a system consisting of two two-atom pairs located a distance  $0.1\lambda$  apart; the two atoms forming one pair are still separated by  $\Delta r = 0.02\lambda$ . Only the first two-atom pair is initially excited, equally in its fast and dark states. We set the equilibrium conditions for the populations of the four  $m = -1$  states (i.e.,  $|aa\rangle|1,0\rangle$ ,  $|aa\rangle|0,0\rangle$ , etc.) to  $1/4$  and that of the  $|aa\rangle|aa\rangle$  ground state to zero. The black curves show the time evolution of the relevant populations for  $\Gamma T_1 = \Gamma T_2 = 10$ , while the red and blue curves show that of the ground state for  $\Gamma T_2 = 1$  and  $0.1$ , respectively;  $T_1$  is unchanged. Although the increased decoherence reduces the energy trapping efficiency from  $\approx 0.6$  to  $\approx 0.5$ , energy trapping still occurs.

The black curves show the time evolution of the corresponding populations for  $\Gamma T_1 = \Gamma T_2 = 10$  when only the first two-atom pair is initially excited, equally in its fast and dark states (i.e., we set  $\langle 1,0|\langle aa|\hat{\rho}|1,0\rangle|aa\rangle = \langle 0,0|\langle aa|\hat{\rho}|0,0\rangle|aa\rangle = 1/2$  and all other populations and coherences to zero). We set the equilibrium conditions for the populations of the four  $m = -1$  states (i.e.,  $|aa\rangle|1,0\rangle$ ,  $|aa\rangle|0,0\rangle$ , etc.) to  $1/4$  and that of the  $|aa\rangle|aa\rangle$  ground state to zero. It is interesting to see how the emission of a photon by the first pair is followed by its absorption by the second, with like-states (e.g.,  $|aa\rangle|1,0\rangle$  and  $|1,0\rangle|aa\rangle$ ) thermalizing to the same steady-state value because of their shared decay rate. Most importantly, the ground state settles to an occupation probability of approximately  $0.4$  leading to an energy trapping efficiency  $\eta \simeq 0.55$ .

The effect of the dephasing time-scale is also depicted in the figure with the red and blue curves for the population of the  $|aa\rangle|aa\rangle$  ground state when  $\Gamma T_2 = 1$  and  $0.1$ , respectively;  $T_1$  is unchanged. It is found, as could be expected, that increased decoherence (i.e., a lower  $T_2$ ) reduces the energy trapping efficiency, but it does not eradicate the effect. Rather, decoherence tends to render the two pairs more uncorrelated.

Figure 4 shows the intensities (normalized to  $\hbar\omega_0\Gamma$ ) for the single-atom, and the two- and four-atom cases of Figures 2 and 3 when  $\Gamma T_1 = \Gamma T_2 = 10$ . While equilibrium conditions have enabled the trapping of energy in the long run, they also bring a non-zero steady-state intensity in all cases. This is not surprising since, as discussed above, equilibrium forces the establishing of non-zero steady-state populations. The systems then radiate in this regime at intensities proportional to the sum of the products of the populations and their transitions rates (see equation A11).

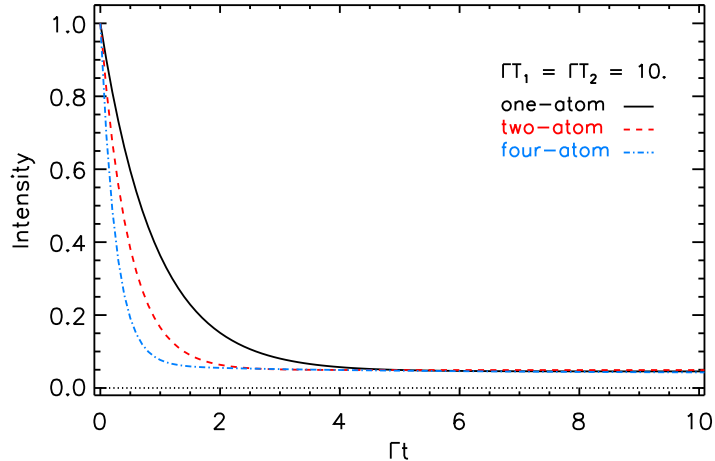


**Fig. 4** Intensities (normalized to  $\hbar\omega_0\Gamma$ ) for the single-atom, and the two- and four-atom cases of Figures 2 and 3 when  $\Gamma T_1 = \Gamma T_2 = 10$ . While equilibrium conditions have enabled the trapping of energy in the long run, they also bring a non-zero steady-state intensity in all cases. Subradiance and energy trapping are apparent from the narrower profiles of the transient intensities for the two- and four-atom systems over the single-atom case.

Subradiance and energy trapping are also apparent in Figure 4 from the shorter time-scales (i.e., narrower profiles) of the transient intensities for the two- and four-atom systems over the single-atom case. But it should be kept in mind that these results all rest on the fact that  $k\Delta r \ll 1$  for the close pairs of atoms. These are not common conditions in the interstellar medium. It would thus appear that a many-atom system would behave in the same manner as a single-atom whenever  $k\Delta r \gg 1$ .

There is, however, another way toward efficient energy trapping. As was observed earlier, environmental conditions can sometimes favor the realization of specific radiation modes. In such cases, radiation can become coherent and transition rates can approach those of the small sample systems (see equations 5-8 or A13-A16).

### 2.3 Superabsorption, coherence and triggered subradiance

Extending the analysis of Sec. 2.2 would quickly become prohibitive for even a moderate number of atoms. Furthermore, we have limited ourselves to transitions between the ground and first excited states. Realistic conditions would require initiating the system at higher internal energy levels. In order to generalize our analysis we now move to the framework of the Maxwell-Bloch equations (MBE), which are presented in Appendix C.

We now study the propagation of an incident radiation field on a slab composed of an atomic gas, similar to what is often done in elementary radiative transfer analysis in astrophysics [23]. This will allow us to compare the outcome of our analysis with well-known results. The MBE are perfectly suited for this problem, being one-dimensional in nature. We will also investigate effects the incident field will have on the radiation emanating from within the gas itself. For a magnetic dipole transition, such as the



atomic hydrogen 21 cm line, the MBE allow us to follow the temporal evolution of three quantities as a function of position  $z$  and the retarded time  $\tau = t - z/c$ : the differential density  $n_- = n_b - n_a$ , with  $n_a$  and  $n_b$  are the number densities of atoms in the lower and upper levels<sup>2</sup>, respectively, the magnetization  $M^+$  and the magnetic field  $B^+$ . Our MBE include relaxation and dephasing time-scales  $T_1$  and  $T_2$ , as well as a thermal equilibrium condition enforced through a corresponding differential density  $n_-^{\text{eq}} = n_b^{\text{eq}} - n_a^{\text{eq}} < 0$  set by the Boltzmann equation for the population of energy levels at the temperature of the gas  $T_{\text{kin}}$ .

With the incident radiation field propagating along a well-defined direction (i.e., along the  $z$ -axis), we have an example of situations where environmental or external conditions favor one radiation mode over others. Importantly, the interaction between the incident field and the gas will initially elicit superabsorption and favor coherence in subsequent transitions through angular correlation among photons, as discussed in Sec. 2.1. It is therefore expected that the radiation field emanating from, and propagating within, the gas itself will also take the same form as that induced by the incident field and be limited to the same radiation mode as the incident field (see equation C32). This effect could be termed *triggered subradiance* as it is in some ways similar to what is observed for triggered superradiance. As experimentally verified by [24], for example, the injection of an incident field at the entrance of a superradiance system will enhance the intensity in the corresponding radiation mode at the expense of all others (including the one where superradiance would naturally occur in the absence of the incident field). While here the incident field is attenuated instead of being amplified, its associated radiation mode will be favored in a similar manner.

Hence, we will subject the system to two independent stimuli: *i*) the aforementioned incident magnetic field  $B_0$ , which effectively serves as a boundary condition at the input  $z = 0$  of the system, and *ii*) initial internal quantum fluctuations throughout the system modeled as an initial magnetization. Since phase coherence is expected for the radiation field, we focus our analysis on a cylinder of cross-section area  $A = \lambda L$ , with  $L$  the length of the cylinder and  $\lambda$  the wavelength of radiation [20] (see Appendix C).

### 2.3.1 Response to incident radiation

**Linear regime.** The general solution of the MBE requires numerical computations. It is, however, possible to provide analytical solutions in the linear regime (i.e., weak radiation intensity) where  $n_- = n_-^{\text{eq}}$ . We show in Appendix C.2 that the magnetic field resulting from the response of the gas to an incident field of amplitude  $B_0$  is

$$B^+(z, \tau) = B_0 \left\{ e^{-\alpha z/2} + \frac{\alpha}{2} e^{-\tau/T_2} \left[ e^{-\alpha z/2} \star J_0 \left( 2\sqrt{\frac{z\tau}{LT_R}} \right) \right] \right\}, \quad (12)$$

where  $J_p(x)$  is the Bessel function of the first kind and order  $p$ , while ‘ $\star$ ’ stands for a (spatial) convolution. The two terms on the right-hand side consist of the steady-state

---

<sup>2</sup>From now on we use lower  $n$ 's for densities and capital  $N$ 's for numbers of particles.

and transient responses, respectively, with the absorption coefficient generally defined as (i.e., for any density  $n_-$ )

$$\begin{aligned}\alpha &= \frac{\mu_0 \omega_0 \mu^2 T_2 |n_-|}{\hbar c} \\ &= \frac{2T_2}{LT_R},\end{aligned}\tag{13}$$

where  $\mu_0$  is the permeability of vacuum and  $\mu$  the magnitude of the transition's magnetic dipole moment. In the last equation we have introduced the superabsorption time-scale (defined at equilibrium)

$$T_R = \frac{8\pi}{3\lambda^2 |n_-^{\text{eq}}| L\Gamma},\tag{14}$$

which has exactly the same form as the superradiance time-scale, except for the fact that in our case  $n_-^{\text{eq}} < 0$  [5, 19, 20].

As we will soon be interested in the duration of the transient response of the system when  $T_2 \ll T_R$ , we note that in this limit the evolution time-scale of the system is (see Appendix C.2)

$$T_{\text{tr}} \approx T_2 \left( 1 + \sqrt{\frac{zT_2}{LT_R}} \right)^{-1}.\tag{15}$$

The transient signal thus dies out on a time-scale of the order of  $T_{\text{tr}}$ .

**Steady-state solution.** It is also instructive to study the steady-state response for more general conditions, i.e., without limiting ourselves to the linear regime. Doing so, we readily find

$$n_- = \frac{n_-^{\text{eq}}}{1 + I/I_{\text{sat}}}\tag{16}$$

$$\frac{dI}{dz} = -\alpha I,\tag{17}$$

where the intensity  $I = cB^+B^-/2\mu_0$  and the saturation intensity

$$I_{\text{sat}} = \frac{\hbar^2 c}{8\mu_0 \mu^2 T_1 T_2}.\tag{18}$$

The steady-state solution leads to relations (i.e., equations 13 and 16-18) that have exactly the same form as the maser equations with, again, the difference that  $n_- < 0$  [2, 5]. Accordingly, two regimes are identified for the intensity.

In the linear regime, when  $I \ll I_{\text{sat}}$ , we find that  $n_-(z, \tau) = n_-^{\text{eq}}$  and

$$I(z) = I_0 e^{-\alpha z}\tag{19}$$

with  $I_0 = c|B_0|^2/2\mu_0$  and  $\alpha$  a constant (i.e., with  $n_- = n_-^{\text{eq}}$  in equation 13). This solution is the same as found in the steady-state component of equation (12), and is of a similar form as Beer's law when  $\alpha$  replaced by [25]

$$\alpha_B = \frac{3}{4} |n_-^{\text{eq}}| \lambda^2 \Gamma \phi(\omega) \quad (20)$$

for a two-level system (i.e., no degeneracies). In this relation,  $\phi(\omega)$  is the normalized atomic distribution in frequency (i.e.,  $\int \phi(\omega) d\omega = 1$ ).

A comparison of equations (13) and (20) reveals that

$$\alpha = \alpha_B T_2 \delta\omega \quad (21)$$

with  $\delta\omega$  the spectral extent of  $B^+(z, \tau)$  as it propagates through the gas. This quantity is the reciprocal of the transient response time-scale given in equation (15). We then find

$$\alpha \approx \alpha_B \left( 1 + \sqrt{\frac{z T_2}{L T_R}} \right). \quad (22)$$

for  $T_2 \ll T_R$ .

We uncover the important result that Beer's law holds strictly only under conditions where  $T_2 \rightarrow 0$ , i.e., in the limit of complete decoherence/dephasing. In the opposite limit when  $T_2 \gg T_R$ , we have  $\delta\omega \sim T_R^{-1}$ ,  $\alpha = \alpha_B T_2 / T_R$  and find, just as importantly, that the density of the gas determined with Beer's law can be overestimated when coherence is present.

The saturated regime when  $I \gg I_{\text{sat}}$  will be considered in more details in a future publication. But we note its solution

$$I(z) = I_0 - \frac{|n_-^{\text{eq}}| \hbar \omega_0}{8 T_1} z \quad (23)$$

for  $z < z_{\text{sat}}$ , where  $z_{\text{sat}}$  is the location where  $I = I_{\text{sat}}$ . This regime is entirely neglected when Beer's law is solely considered.

An example steady-state solution obtained with the MBE is shown in Figure 5 with the intensity plotted as a function of the position within the gas. The shape of the intensity curve is reminiscing, and practically a mirror image, of the one obtained for masers when  $n_- > 0$  (see Fig. 4 in [5]).

**Linear regime response – The 21 cm line.** A slab of atomic hydrogen gas of length  $L \simeq 1.5$  pc at thermal equilibrium with a density of  $1 \text{ cm}^{-3}$  and a temperature  $T_{\text{kin}} = 10$  K is now considered (see Sec. 4). This approximately corresponds to typical mass densities measured in dark matter halos [26, 27], while we assume the gas to be cold. The response of the system to a constant incident radiation field  $B_0 = 1 \times 10^{-23}$  T, as numerically computed with the MBE (i.e., equations C28-C30), is shown in Figure 6. This corresponds to an incident intensity approximately five orders of magnitude lower than the saturation intensity  $I_{\text{sat}}$ , which ensures that we are well into the linear

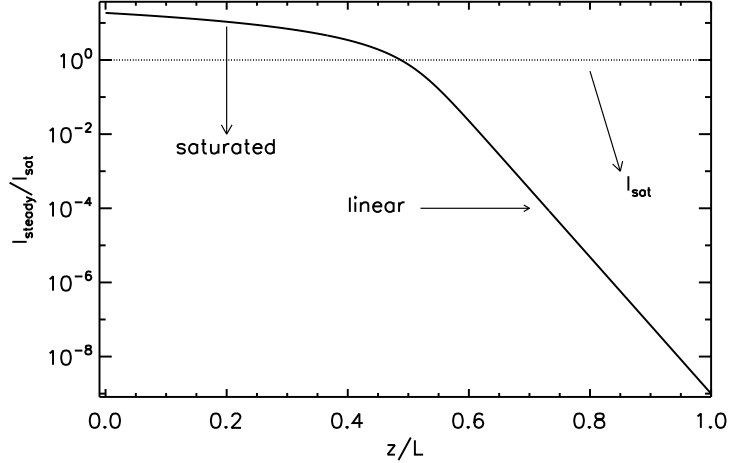


**Fig. 5** Example steady-state intensity as a function of position along the optical path in the gas. This result was obtained with the MBE (i.e., equations C28-C30). The linear and saturated regimes are indicated, as well as the saturation intensity  $I_{\text{sat}}$ .

regime. The precise intensity level is irrelevant to our discussion, as long as we remain in the linear regime.

The left panel of Figure 6 shows the temporal evolutions of the radiation intensity (normalized to  $I_{\text{sat}}$ ; *top*) and the magnetic field (*bottom*). A broken curve in red corresponding to equation (12) is plotted on top of that obtained from numerical computations using the MBE for the magnetic field (in black); there is perfect agreement between the two. The (constant) density  $n_-$  (in black) and pump  $\Lambda_n$  (in cyan; using the vertical scale on the right; *top*) and the magnetization (in units of Bohr magneton  $\mu_B$  per cubic centimeter; *bottom*) are displayed in the right panel. We note that the mean distance between neighboring cooperating atoms is  $\Delta r \approx 670\lambda$  and  $T_2 \simeq 16T_R$ , which implies that coherence can be sustained in the system under these conditions.

It is interesting to note that at  $\tau = 0$  the incident magnetic field is transmitted unattenuated at  $z = L$  (or any other position) no matter how large  $L$  is. Thereafter, superabsorption defines the transient response to greatly reduce the intensity on a time-scale  $\approx T_R$  and in an oscillatory manner reminiscing of superradiance systems. According to our previous discussion, the steady-state regime settles afterwards to an intensity diminished by a factor  $e^{-\alpha L}$ , where  $\alpha L = 2T_2/T_R \simeq 32$  from equation (13). Such signal would therefore be detected as a deep and narrow absorption line ( $\approx 0.5 \text{ km s}^{-1}$  in width) against the background radiation.

### 2.3.2 Response to initial fluctuations

As shown in Appendices C.1 and C.2, the linear regime response of the system to initial internal fluctuations  $M^+(z, 0) = n_-^{\text{eq}} \mu \theta_0 / 2$  within the gas, with  $\theta_0$  the initial

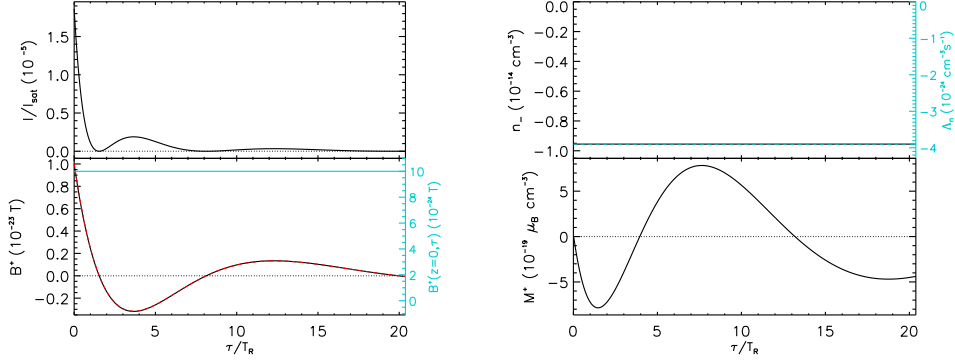


**Fig. 6** *Left*: Temporal evolutions of the radiation intensity (*top*) and magnetic induction field (*bottom*) of the 21 cm line for an atomic hydrogen gas at a temperature of 10 K and length  $L \simeq 1.5$  pc. We set  $T_1 = T_2 \simeq 16 T_R$  and the intensity is normalized to the saturation intensity  $I_{\text{sat}}$  given in equation (18). In the bottom panel, the incident magnetic field's amplitude is shown in cyan (using the vertical scale on the right), while a broken curve in red corresponding to equation (12) is plotted on top of that obtained from numerical computations (in black) using the MBE. *Right*: Temporal evolution of the density  $n_-$  in black with the pump  $\Lambda_n = n_-^{\text{eq}}/T_1$  in cyan (using the vertical scale on the right; *top*) and the magnetization (*bottom*). The density is limited to the spectral extent of the signal (i.e.,  $T_R^{-1}$ ) and corresponds to a total density of  $1 \text{ cm}^{-3}$  for a gas at a temperature of 10 K. The mean distance between neighboring cooperating atoms is  $\Delta r \approx 670\lambda$  and  $T_R = 1.5 \times 10^8 \text{ s} \simeq 4.3 \times 10^{-7} / \Gamma$ .

“rising” angle, is expressed as

$$B^+(z, \tau) = -i \frac{\hbar \theta_0}{2\mu T_R} e^{-\tau/T_2} \frac{z}{L} \sqrt{\frac{LT_R}{z\tau}} J_1\left(2\sqrt{\frac{z\tau}{LT_R}}\right). \quad (24)$$

Studying the behavior of  $J_1(2\sqrt{x})/\sqrt{x}$  reveals that the amplitude of the field corresponding to the initial fluctuations in magnetization is transmitted without amplification/absorption to  $z = L$  at  $\tau = 0$ . This response is linear in  $z$  and therefore coherent (i.e., the intensity is proportional to  $z^2$ ). At a given position, the field (and the corresponding intensity) displays a weak oscillatory temporal behavior with a period scaling with  $T_R$ , but damped on the dephasing time-scale  $T_2$ . Importantly, we find that the magnetic field is zero in the steady-state.

We show in Figure 7 the response to these internal fluctuations for the same system as when studying the propagation of an incident radiation field. In the left panel the intensity is normalized to that expected from a gas radiating non-coherently (denoted by  $I_{\text{nc}}$ ; see Appendix C.3). The curve for the normalized intensity is reminiscent of those found in Figure 4 for the simple two- and four-atom systems discussed in Sec. 2.2 using the master equation. Here, however, we have  $\sim 10^{27}$  cooperating atoms in total contained in the system, which in comparison leads to an extreme level of subradiance.

More precisely, at  $\tau = 0$  the system's intensity is at a level similar to what is expected from a non-coherent gas (i.e.,  $I = 0.25 I_{\text{nc}}$ ), but it only radiates for a duration  $\approx T_R$ . To that effect, we should emphasize that  $\Gamma T_R \simeq 4.3 \times 10^{-7}$ . In comparison, for the 21 cm line the non-coherent transient intensity for non-cooperating atoms would last on the order of  $\Gamma^{-1} \sim 10^7$  yr, whereas  $T_R \sim 5$  yr. This implies that almost the

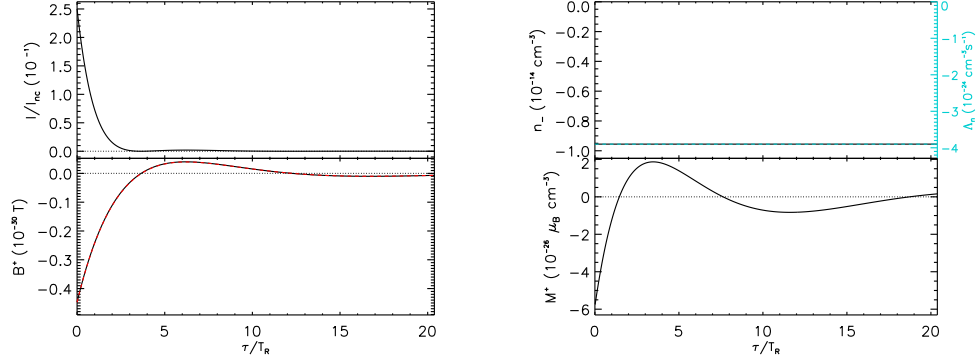


**Fig. 7** *Left:* Radiation intensity (*top*) and (the imaginary part of) the magnetic field (*bottom*) of the 21 cm line for the same atomic hydrogen gas as in Figure 6 in response to initial internal fluctuations. The intensity is normalized to that expected from a gas radiating non-coherently under the same conditions. A broken curve in red corresponding to equation (24) is plotted on top of that obtained from numerical computations (in black) using the MBE. *Right:* Temporal evolution of the density  $n_-$  in black with the pump  $\Lambda_n = n_-^{\text{eq}}/T_1$  in cyan (using the vertical scale on the right; *top*) and the magnetization (*bottom*).

totality of the available energy is locked within the atomic population, which is almost entirely in dark states since the fast states are quickly depleted during the transient regime.

Unlike the two- and four-atom systems in Figure 4, the steady-state intensity is zero despite having a significant fraction (almost half) of the atoms in the excited state. The combination of the widespread entanglement of atoms and coherence in our system suppresses the intensity in the steady-state regime. We therefore find that the gas becomes completely dark after a very short time.

### 3 Discussion

If entanglement naturally results from the interaction between the atoms composing the gas and the ambient electromagnetic field, coherence can only happen under certain conditions. As reviewed in Secs. 2.1 and 2.2, close proximity between atoms (i.e., separations much shorter than  $\lambda$ ; the small sample limit) ensures coherence for all radiation modes. The manifestation of this coherence will take different forms depending on the initial conditions. For example, superradiance will ensue when the gas is initially hosting a population inversion. Otherwise, at thermal equilibrium, for example, the initial occupation of slow and dark states leads to subradiance. Importantly, dark states are responsible for the trapping of energy and the suppression of radiation in the steady-state. However, close proximity between cooperating radiators is unlikely to be common in astrophysical media and the trapping of radiation is negated under such conditions, as energy escapes through non-coherent radiation modes.

Equilibrium conditions set the population of slow and dark states, and will naturally stop their gradual decay in the steady-state. These features render equilibrium

essential to achieving significant levels of subradiance. However, this comes at the cost of a non-zero steady-state intensity (see Figure 4).

Close proximity between atoms is not the only way to achieve energy trapping. As is evident from the transition rates for the two-atom system (see equations 7-8 and A15-A16), no matter how large the separation between atoms, coherence can be achieved through angular correlation between emitted/absorbed photons. This will be realized whenever one mode of radiation (or a few) is favored over the others. This can happen whenever some form of anisotropy is present, whether in the geometry of the system or the ambient physical conditions (e.g., accentuated velocity coherence along a well-defined direction). Although these forms of anisotropy are also applicable to the problem of the atomic hydrogen 21 cm line analyzed in Sec. 2.3, we found that another scenario is likely to be efficient in that respect.

In our analysis of the 21 cm line in Sec. 2.3, we purposely chose a gas density that is in line with measurements in dark matter halos. For the matter contained in these environments, the main source of anisotropy comes in the form of the radiation field emanating from the host galaxy. As then mentioned, the incidence of this field will effectively select one mode for the propagation of radiation within the halo. It is expected that superabsorption of the incident field will elicit coherence in subsequent transitions in the gas through angular correlation among photons. As a consequence, extreme subradiance, leading to a complete darkening of the gas, takes place within a few years even at a mean separation  $\Delta r \approx 670\lambda$  between closest neighbors. As far as emission properties are concerned, this atomic hydrogen gas is invisible and effectively behaves like dark matter. This darkening effect may therefore possibly account for the dark matter known to exist in these environments.

However, is the suppression of radiation in a given transition through triggered subradiance sufficient for the corresponding atomic species to be considered dark? In other words, what about all the other transitions pertaining to this atom?

Entanglement is not a property that is unique to a specific transition. That is, it is always possible to use the symmetry of the Hamiltonian to determine proper states for the problem at hand. The forms of these symmetry-adapted states are the same for all energy levels. For example, if equations (1)-(4) apply to the states pertaining to the 21 cm transition for two entangled atoms, then similar looking states will also apply for, say, the Lyman- $\alpha$  or other hydrogen lines. In other words, entanglement is a global property of the atom. Coherence, however, is not and needs to be assessed on a transition by transition basis.

For our analysis of the 21 cm line for a gas at a density  $n_{-}^{\text{eq}} = 1 \text{ cm}^{-3}$  and temperature  $T_{\text{kin}} = 10 \text{ K}$  these considerations have no bearing on the outcome since all other lines (e.g., Lyman- $\alpha$ ) will remain essentially unexcited. The gas as a whole will thus appear dark in the steady-state on the account of the 21 cm line alone. While we only studied this specific example, similar conclusions may be reached when considering other environments with differing gas densities and temperatures, or other atomic/molecular species. It also follows that this darkening effect, which also relies on the presence of anisotropic radiation, should be closely correlated with the presence of “luminous” matter, as is the case for dark matter [27].

We also studied the propagation of an incident radiation field at 21 cm in the same atomic hydrogen gas. Interestingly, we found that Beer’s law, commonly used to quantify the attenuation in intensity as a function of position, is an approximation that holds only under complete decoherence/dephasing (i.e., in the limit  $T_2 \rightarrow 0$ ) in the linear regime. It follows that the amount of attenuation could exceed expected levels in situations where coherence exists in the gas. Furthermore, the existence of the saturated regime is completely missed when only Beer’s law is considered.

We are then led to a picture where our “dark” hydrogen gas (in emission) would also appear more opaque (or more optically thick) in its absorption lines against the background source responsible for the incident radiation. However, it would otherwise be completely transparent to radiation at wavelengths alien to the hydrogen atom, as expected from dark matter. For a cold gas as the one considered in our analysis, these lines would appear as narrow absorption features, such as those commonly detected in observations of the interstellar medium [28], the Galactic halo [29], the Galactic disk [30] and external galaxies [31].

Another important property of our darkened atomic hydrogen gas is discussed in Appendix D. There, we calculate the cross-section for high-speed collisions between two two-atom systems (i.e., when the kinetic energy is far greater than the transition excitation energy  $\hbar\omega_0$ ), both being entangled as discussed in Sec. 2.1. Interestingly, it is found that in such circumstances the collision cross-section will likely vanish because of destructive interference due to the entangled nature of the states the systems find themselves in after the transient regime. Although this analysis needs to be generalized, this result is consistent with astronomical observations of the so-called bullet cluster (with collision speeds on the order of  $10^3 \text{ km s}^{-1}$ ) and similar objects [32]. These observations put a constraint on the ratio of the collision cross-section to the mass of a purported dark matter (point) particle to  $\sigma/M \lesssim 1 \text{ cm}^2 \text{ g}^{-1}$  [27]. Although the corresponding figure for atomic hydrogen is  $\sim 10^9 \text{ cm}^2 \text{ g}^{-1}$ , it does not apply in our case. Our analysis does not suggest that atomic hydrogen is a dark matter particle, but rather that the cooperative behavior of a large number of entangled hydrogen atoms is consistent with what is expected for dark matter. While individual atoms may still collide, entangled systems of atoms will be essentially collisionless.

Finally, we should make a few observations concerning our model based on the MBE. First, we used the Arecchi-Courtens condition to set the length scale of a coherent entity within the gas [33]. In superradiance systems, for example, this is applicable to cases where the pump responsible for the population inversion is transverse, i.e., it affects the gas simultaneously at all positions. When this happens, regions separated by a distance  $L > cT_R$  will evolve on a time-scale ( $T_R$ ) shorter than that needed for their interaction ( $L/c$ ) and, therefore, cannot work cooperatively. In our case, thermal equilibrium is set by the pump and one would therefore expect the Arecchi-Courtens condition to apply. However, the favoring of a single radiation mode, through which the photon angular correlation and coherence are set, can only happen when upstream photons reach atoms located further down along the optical path. This is akin to the effect of a longitudinal pump, in which case the Arecchi-Courtens condition would not apply [20]. This would then relax any restriction on the coherent length in the gas



and allow for lower values of  $T_R$ , and potentially broaden the applicability and the strength of the darkening effect.

On the other hand, the use of the MBE renders it difficult to investigate situations where coherence and the darkening effect cannot be established. This is because the selection of a single radiation mode is inherent in the model (see equations C31-C32). The only manner coherence can be impeded is, therefore, through the lowering of the dephasing time-scale  $T_2$ . But for subradiance the impact of a lower  $T_2$  is limited to the dampening of the signal.

This limited effect of dephasing in our system stems from the fact our model is one-dimensional. For example, the darkening effect clearly cannot proceed for a more-or-less spherical cloud of gas when the ambient field is not sufficiently anisotropic to ensure the selection of one (or a few) radiation mode. To numerically test this scenario, one would need a three-dimensional generalization of the MBE to allow for differing boundary conditions (i.e., different types of incident field) and geometries for the cloud of gas. This would also permit the investigation of the effect of dephasing and decoherence when a large number of radiation modes are available. This may reveal the lack of a darkening, or some limitation of it, for sufficiently low values of  $T_2$ .

## 4 Methods

For the atomic hydrogen slab of density  $1 \text{ cm}^{-3}$  and temperature  $T_{\text{kin}} = 10 \text{ K}$  considered in Secs. 2.3.1 and 2.3.2, thermal motions bring an average time-scale between collisions of about  $2.5 \times 10^9 \text{ s}$ , which we ascribe to  $T_2$ . Since we are considering radiation from the 21 cm line, which has an excitation temperature  $T_{21 \text{ cm}} \simeq 0.068 \text{ K} \ll 10 \text{ K}$ , we set, for simplicity,  $T_1 \approx T_2 = 2.5 \times 10^9 \text{ s}$  (i.e., we assume that inelastic and elastic collisions happen at similar rates and are the sole sources of relaxation and dephasing in the gas, respectively).

Because we expect the linear regime response of the system to happen on the superabsorption time-scale  $T_R$  (see equations 12 and 24) it follows that only a fraction of the atomic population can act cooperatively in the process. That is, given the spectral breadth  $\Delta\omega \sim \omega_0 \Delta v/c$  associated with thermal motions (of characteristic speed  $\sim \Delta v$ ) the density entering our equations is  $1 \text{ cm}^{-3}/T_R \Delta\omega$ . In accordance with the Arecchi-Courtens condition [33], we fixed the thickness of the slab to  $L = cT_R$ , which corresponds to the maximum length of a coherent region when the excitation happens simultaneously over the whole sample (see the corresponding discussion in Sec. 3). Using equation (14) and the Boltzmann equation for the population of energy levels we arrive at  $n_-^{\text{eq}} = 9.6 \times 10^{-15} \text{ cm}^{-3}$ ,  $L = 4.5 \times 10^{18} \text{ cm} \simeq 1.5 \text{ pc}$  and  $T_R = 1.5 \times 10^8 \text{ s} = 4.3 \times 10^{-7}/\Gamma^{-1}$ , with  $\Gamma \simeq 2.9 \times 10^{-15} \text{ s}^{-1}$  for the 21 cm line. We therefore set a constant ‘‘pump’’  $\Lambda_n = n_-^{\text{eq}}/T_1$  to enforce thermal equilibrium and keep  $n_- = n_-^{\text{eq}}$  at all times (see equation C28).

Given a set of initial and boundary conditions for  $n'$ ,  $M^+$  and  $B^+$ , as well as the values for  $T_1$ ,  $T_2$  and  $n'_{\text{eq}}$ , the MBE (i.e., equations C28-C30) are solved by numerical integration using a fourth-order Runge-Kutta method. We compute the evolution of the system of length  $L$  up to a retarded time  $\tau_{\text{max}}$  by moving forward in  $\tau$  for a given position  $z_k$  ( $k$  is an integer) with  $n'$  and  $M^+$  evaluated at the next grid point in  $\tau$ , and

$B^+$  at the next spatial point  $z_{k+1}$ . This process is repeated for  $z = z_{k+1}$  and  $\tau = 0$  once  $\tau = \tau_{\max}$  is reached, and so on until  $z_k = L$  [10, 34].

## References

- [1] Dicke, R.H.: Coherence in spontaneous radiation processes. *Phys. Rev.* **93**, 99–110 (1954) <https://doi.org/10.1103/PhysRev.93.99>
- [2] Feld, M.S., MacGillivray, J.C.: Superradiance. *Topics in Current Physics* **21**, 7–57 (1980) [https://doi.org/10.1007/978-3-642-81495-2\\_2](https://doi.org/10.1007/978-3-642-81495-2_2)
- [3] Skribanowitz, N., Herman, I.P., MacGillivray, J.C., Feld, M.S.: Observation of Dicke Superradiance in Optically Pumped HF Gas. *Phys. Rev. Lett.* **30**, 309–312 (1973) <https://doi.org/10.1103/PhysRevLett.30.309>
- [4] Weaver, H., Williams, D.R.W., Dieter, N.H., Lum, W.T.: Observations of a Strong Unidentified Microwave Line and of Emission from the OH Molecule. *Nature* **208**(5005), 29–31 (1965) <https://doi.org/10.1038/208029a0>
- [5] F. Rajabi and M. Houde: Astronomical masers and Dicke’s superradiance. *Mon. Not. R. Astron. Soc.* **494**(4), 5194–5206 (2020) <https://doi.org/10.1093/mnras/staa1067> [arXiv:2004.07327](https://arxiv.org/abs/2004.07327) [astro-ph.GA]
- [6] F. Rajabi and M. Houde: Dicke’s Superradiance in Astrophysics. I. The 21 cm Line. *Astrophys. J.* **826**(2), 216 (2016)
- [7] F. Rajabi and M. Houde: Dicke’s Superradiance in Astrophysics. II. The OH 1612 MHz Line. *Astrophys. J.* **828**(1), 57 (2016)
- [8] F. Rajabi and M. Houde: Explaining recurring maser flares in the ISM through large-scale entangled quantum mechanical states. *Science Advances* **3**, 1601858 (2017) <https://doi.org/10.1126/sciadv.1601858>
- [9] Houde, M., Mathews, A., Rajabi, F.: Explaining fast radio bursts through Dicke’s superradiance. *Mon. Not. R. Astron. Soc.* **475**, 514–522 (2018) <https://doi.org/10.1093/mnras/stx3205>
- [10] Houde, M., Rajabi, F., Gaensler, B.M., Mathews, A., Tranchant, V.: Triggered superradiance and fast radio bursts. *Mon. Not. R. Astron. Soc.* **482**(4), 5492–5499 (2019) <https://doi.org/10.1093/mnras/sty3046> [arXiv:1810.04364](https://arxiv.org/abs/1810.04364) [astro-ph.HE]
- [11] Rajabi, F., Houde, M., Bartkiewicz, A., Olech, M., Szymczak, M., Wolak, P.: New evidence for Dicke’s superradiance in the 6.7 GHz methanol spectral line in the interstellar medium. *Mon. Not. R. Astron. Soc.* **484**(2), 1590–1597 (2019) <https://doi.org/10.1093/mnras/stz074> [arXiv:1810.04365](https://arxiv.org/abs/1810.04365) [astro-ph.GA]
- [12] Rajabi, F., Houde, M., MacLeod, G.C., Goedhart, S., Tanabe, Y., van den Heever,

- S.P., Wyenberg, C.M., Yonekura, Y.: Modelling of the multitransition periodic flaring in G9.62+0.20E. *Mon. Not. R. Astron. Soc.* **526**(1), 443–455 (2023) <https://doi.org/10.1093/mnras/stad2671> arXiv:2303.08793 [astro-ph.GA]
- [13] Houde, M., Rajabi, F., MacLeod, G.C., Goedhart, S., Tanabe, Y., van den Heever, S.P., Wyenberg, C.M., Yonekura, Y.: Variability, flaring and coherence – the complementarity of the maser and superradiance regimes. In: Hirota, T., Imai, H., Menten, K., Pihlström, Y. (eds.) *Cosmic Masers: Proper Motion Toward the Next-Generation Large Projects*. IAU Symposium, vol. 380, pp. 399–413 (2024). <https://doi.org/10.1017/S1743921323002764>
- [14] Rashidi, T., Anari, V., Bartkiewicz, A., Wolak, P., Szymczak, M., Rajabi, F.: Superradiance and Periodic 6.7 GHz Methanol Flaring in G22.356+0.066. arXiv e-prints, 2409–09209 (2024) <https://doi.org/10.48550/arXiv.2409.09209> arXiv:2409.09209 [astro-ph.HE]
- [15] Pavolini, D., Crubellier, A., Pillet, P., Cabaret, L., Liberman, S.: Experimental evidence for subradiance. *Phys. Rev. Lett.* **54**, 1917–1920 (1985) <https://doi.org/10.1103/PhysRevLett.54.1917>
- [16] Guerin, W., Araújo, M.O., Kaiser, R.: Subradiance in a Large Cloud of Cold Atoms. *Phys. Rev. Lett.* **116**(8), 083601 (2016) <https://doi.org/10.1103/PhysRevLett.116.083601> arXiv:1509.00227 [physics.atom-ph]
- [17] Rubin, Vera C. and Ford, Jr., W. Kent: Rotation of the Andromeda Nebula from a Spectroscopic Survey of Emission Regions. *Astrophys. J.* **159**, 379 (1970) <https://doi.org/10.1086/150317>
- [18] Dicke, R.H.: The coherence brightened laser. *Quantum electron.* **1**, 35–54 (1964)
- [19] MacGillivray, J.C. and Feld, M.S.: Theory of superradiance in an extended, optically thick medium. *Phys. Rev. A* **14**(3), 1169–1189 (1976) <https://doi.org/10.1103/PhysRevA.14.1169>
- [20] M. Gross and S. Haroche: Superradiance: An essay on the theory of collective spontaneous emission. *Phys. Rep.* **93**(5), 301–396 (1982)
- [21] Yang, Daeho and Oh, Seung-hoon and Han, Junseok and Son, Gibeom and Kim, Jinuk and Kim, Junki and Lee, Moonjoo and An, Kyungwon: Realization of superabsorption by time reversal of superradiance. *Nature Photonics* **15**(4), 272–276 (2021) <https://doi.org/10.1038/s41566-021-00770-6> arXiv:1906.06477 [quant-ph]
- [22] Ficek, Z. and Tanaś, R.: Entangled states and collective nonclassical effects in two-atom systems. *Phys. Rep.* **372**(5), 369–443 (2002) [https://doi.org/10.1016/S0370-1573\(02\)00368-X](https://doi.org/10.1016/S0370-1573(02)00368-X) arXiv:quant-ph/0302082 [quant-ph]

- [23] Rybicki, George B. and Lightman, Alan P.: Radiative Processes in Astrophysics. Wiley, New York (1979)
- [24] Carlson, N.W., Jackson, D.J., Schawlow, A.L., Gross, M., Haroche, S.: Super-radiance triggering spectroscopy. *Optics Communications* **32**(2), 350–354 (1980) [https://doi.org/10.1016/0030-4018\(80\)90140-6](https://doi.org/10.1016/0030-4018(80)90140-6)
- [25] Houde, M., Lankhaar, B., Rajabi, F., Chamma, M.A.: The generation and transformation of polarization signals in molecular lines through collective anisotropic resonant scattering. *Mon. Not. R. Astron. Soc.* **511**(1), 295–315 (2022) <https://doi.org/10.1093/mnras/stab3806> arXiv:2112.15104 [astro-ph.GA]
- [26] Kafle, P.R., Sharma, S., Lewis, G.F., Bland-Hawthorn, J.: On the Shoulders of Giants: Properties of the Stellar Halo and the Milky Way Mass Distribution. *Astrophys. J.* **794**(1), 59 (2014) <https://doi.org/10.1088/0004-637X/794/1/59> arXiv:1408.1787 [astro-ph.GA]
- [27] Cirelli, M., Strumia, A., Zupan, J.: Dark matter. arXiv e-prints, 2406–01705 (2024) <https://doi.org/10.48550/arXiv.2406.01705> arXiv:2406.01705 [hep-ph]
- [28] Li, D. and Goldsmith, P. F.: HI Narrow Self-Absorption in Dark Clouds. *Astrophysics. J.* **585**(2), 823–839 (2003) <https://doi.org/10.1086/346227> arXiv:astro-ph/0206396 [astro-ph]
- [29] Mohan, R., Dwarakanath, K.S., Srinivasan, G.: A high galactic latitude HI 21 cm-line absorption survey using the GMRT: I. Observations and spectra. *Journal of Astrophysics and Astronomy* **25**(3-4), 143–183 (2004) <https://doi.org/10.1007/BF02702370> arXiv:astro-ph/0410626 [astro-ph]
- [30] Sun, S., Wang, K., Liu, X., Xu, F.: The Formation of Milky Way “Bones”: Ubiquitous HI Narrow Self-absorption Associated with CO Emission. *Astrophysics. J. Lett.* **973**(1), 27 (2024) <https://doi.org/10.3847/2041-8213/ad77ce> arXiv:2409.01895 [astro-ph.GA]
- [31] Yoon, H., Sadler, E.M., Mahony, E.K., Aditya, J.N.H.S., Allison, J.R., Glowacki, M., Kerrison, E.F., Moss, V.A., Su, R., Weng, S., Whiting, M., Wong, O.I., Callingham, J.R., Curran, S.J., Darling, J., Edge, A.C., Ellison, S.L., Emig, K.L., Garratt-Smithson, L., German, G., Grasha, K., Koribalski, B.S., Morganti, R., Oosterloo, T., Péroux, C., Pettini, M., Pimbblet, K.A., Zheng, Z., Zwaan, M., Ball, L., Bock, D.C.-J., Brodrick, D., Bunton, J.D., Cooray, F.R., Edwards, P.G., Hayman, D.B., Hotan, A.W., Lee-Waddell, K., McClure-Griffiths, N.M., Ng, A., Phillips, C.J., Raja, W., Voronkov, M.A., Westmeier, T.: The First Large Absorption Survey in HI (FLASH): II. Pilot Survey data release and first results. arXiv e-prints, 2408–06626 (2024) <https://doi.org/10.48550/arXiv.2408.06626> arXiv:2408.06626 [astro-ph.GA]
- [32] Clowe, D., Bradač, M., Gonzalez, A.H., Markevitch, M., Randall, S.W., Jones, C.,

- Zaritsky, D.: A Direct Empirical Proof of the Existence of Dark Matter. *Astrophys. J.* **648**(2), 109–113 (2006) <https://doi.org/10.1086/508162> arXiv:astro-ph/0608407 [astro-ph]
- [33] F.T. Arecchi and E. Courtens: Cooperative Phenomena in Resonant Electromagnetic Propagation. *Phys. Rev. A* **2**, 1730–1737 (1970) <https://doi.org/10.1103/PhysRevA.2.1730>
- [34] Mathews, A.: The Role of Superradiance in Cosmic Fast Radio Bursts. Honours thesis, The University of Western Ontario (2017)
- [35] Cohen-Tannoudji, C., Diu, B., Laloë, F.: *Mécanique Quantique - Tome I*. CNRS Éditions, Paris (2018)
- [36] I.S. Gradshteyn and I.M. Ryzhik: *Table of Integrals, Series and Products*. Academic Press, Inc, San Diego (1980)
- [37] Haroche, Serge and Raimond, Jean-Michel: *Exploring the Quantum: Atoms, Cavities and Photons*. Oxford University Press, New York (2008)
- [38] Cohen-Tannoudji, C., Diu, B., Laloë, F.: *Mécanique Quantique - Tome II*. CNRS Éditions, Paris (2018)

**Acknowledgements.** We thank J. Cami, B. Lankhaar and A. Mathews for their helpful comments. M.H.’s research is funded through the Natural Sciences and Engineering Research Council of Canada (NSERC) Discovery Grant RGPIN-2024-05242 and the Western Strategic Support for Research Accelerator Success. F.R.’s research is supported by the NSERC Discovery Grant RGPIN-2024-06346. M.H. and F.R. are grateful for the hospitality of Perimeter Institute where part of this work was carried out.

## Author contributions:

M.H. conceptualized the work. Both authors contributed equally to the analysis and the writing of the paper.

## Declarations

The authors declare no competing interest.

**Supplementary information to:**  
**Quantum coherence and the invisible Universe: Subradiance as a dark matter mechanism**

Martin Houde<sup>1\*</sup> and Fereshteh Rajabi<sup>2</sup>

<sup>1\*</sup>Department of Physics and Astronomy, The University of Western Ontario,  
1151 Richmond Street, London, N6A 3K7, Ontario, Canada

<sup>2</sup>Department of Physics and Astronomy, McMaster University,  
1280 Main Street West, Hamilton, L8S 4L8, Ontario, Canada

\*Corresponding author. E-mail: [mhoude2@uwo.ca](mailto:mhoude2@uwo.ca)

Contributing author: [rajabfi@mcmaster.ca](mailto:rajabfi@mcmaster.ca)

**CONTENTS**

Appendix A: Hamiltonian and transition rates	23
Two-atom transition rates from $m = 0$ and superabsorption	24
Energy trapping efficiency for $n$ atoms	25
Appendix B: The master equation	25
Appendix C: The Maxwell-Bloch equations	27
Initial Bloch angle and magnetization	28
Linear regime solutions	30
Non-coherent radiation intensity	31
Appendix D: Collision cross-section	31

## Appendix A Hamiltonian and transition rates

Following Dicke [1] and we express the Hamiltonian for the gas with

$$\hat{H} = \hat{H}_0 + \hbar\omega_0 \sum_j \hat{R}_j^3 + \hat{V}, \quad (\text{A1})$$

where  $\hat{H}_0$  accounts for the translational motions of the atoms' center-of-mass, the second term for their internal energy and  $\hat{V}$  for dipole interactions with the electromagnetic field. For simplicity we approximate the atoms as two-level systems at resonance with each other with an internal energy difference  $\hbar\omega_0$ ; the summation in equation (A1) is on all atoms. That is, if  $|a\rangle$  and  $|b\rangle$  are the lower and upper atomic states, respectively, then for the  $j^{\text{th}}$  atom  $\hat{R}_j^3 = \frac{1}{2}(|b\rangle\langle b| - |a\rangle\langle a|)$ .

For our problem the interaction term reduces to

$$\hat{V} = -i \sum_k \frac{1}{2} \hbar \Omega_k \left( \hat{R}_k^+ \hat{a}_k - \hat{R}_k^- \hat{a}_k^\dagger \right), \quad (\text{A2})$$

where the summation on  $k$  is on the radiation modes, and  $\hat{a}_k$  and  $\hat{a}_k^\dagger$  are the photon annihilation and creation operators. In equation (A2) the Rabi frequency is given by

$$\Omega_k = \frac{2\mu\mathcal{E}_0}{\hbar c} (\boldsymbol{\epsilon}_\mu \cdot \boldsymbol{\epsilon}_k^\perp) \quad (\text{A3})$$

for a magnetic dipole transition, where  $\mu$  and  $\boldsymbol{\epsilon}_\mu$  are the magnitude of the magnetic dipole moment and its associated unit vector (assumed real), while that for the radiation mode's polarization is (also real and) denoted by  $\boldsymbol{\epsilon}_k^\perp$  (i.e.,  $\mathbf{k} = k\boldsymbol{\epsilon}_k$  and  $\boldsymbol{\epsilon}_k \cdot \boldsymbol{\epsilon}_k^\perp = 0$ ). The one-photon electric field is

$$\mathcal{E}_0 = \sqrt{\frac{\hbar\omega_0}{2\epsilon_0\mathcal{V}}} \quad (\text{A4})$$

with  $\epsilon_0$  the permittivity of vacuum and  $\mathcal{V}$  the volume of quantization. We focus on magnetic dipole transitions in view of our application to the atomic hydrogen 21 cm line in Sec. 2.3. For an electrical dipole transition one has to substitute  $\mu \rightarrow dc$  and  $\boldsymbol{\epsilon}_\mu \rightarrow \boldsymbol{\epsilon}_d$  in equation (A3), with  $d$  the magnitude of the electric dipole moment.

The phase-matched raising and lowering operators introduced in equation (A2) are defined by

$$\hat{R}_k^\pm = \sum_j \hat{R}_j^\pm e^{\pm i\mathbf{k}\cdot\mathbf{r}_j} \quad (\text{A5})$$

with  $\mathbf{r}_j$  the position of atom  $j$ . For the single-atom raising and lowering operators we have  $\hat{R}_j^+ = |b\rangle\langle a|$  and  $\hat{R}_j^- = |a\rangle\langle b|$  while, as we assume resonance, we write  $k = |\mathbf{k}| = \omega_0/c$ . For two identical two-level atoms located a distance  $z_0$  from one another (Atom 1 at  $-z_0/2$  and Atom 2 at  $z_0/2$  on the  $z$ -axis), as considered in Sec. 2.1, we have

$$\hat{R}_k^\pm = \hat{R}_1^\pm e^{\mp i\frac{1}{2}kz_0 \cos\theta} + \hat{R}_2^\pm e^{\pm i\frac{1}{2}kz_0 \cos\theta} \quad (\text{A6})$$

with  $\theta$  the angle of  $\mathbf{k}$  relative to the  $z$ -axis.

## A.1 Two-atom transition rates from $m = 0$ and superabsorption

Starting with equations (7)-(8), we can obtain the radiation intensity by integrating these transition rates over  $d\Omega'$ . Setting  $\cos\theta = 0$ , for simplicity, we find

$$\gamma_{1,0_\theta \rightarrow 1,-1} = \Gamma [1 + F(kz_0)] \quad (\text{A7})$$

$$\gamma_{0,0_\theta \rightarrow 1,-1} = \Gamma [1 - F(kz_0)] \quad (\text{A8})$$

with

$$F(kz_0) = \frac{3}{2} \left\{ \left[ 1 - (\epsilon_\mu \cdot \epsilon_z)^2 \right] \frac{\sin(kz_0)}{kz_0} + \left[ 1 - 3(\epsilon_\mu \cdot \epsilon_z)^2 \right] \left[ \frac{\cos(kz_0)}{(kz_0)^2} - \frac{\sin(kz_0)}{(kz_0)^3} \right] \right\} \quad (\text{A9})$$

and

$$\Gamma = \frac{\mu_0 \omega_0^3 \mu^2}{3\pi \hbar c^3} \quad (\text{A10})$$

the single-atom free-space spontaneous emission rate with  $\mu_0$  the permeability of vacuum (for an electric dipole transition we again substitute  $\mu \rightarrow dc$ ).

We consider initial conditions where the states  $|1, 0\rangle_\theta$  and  $|0, 0\rangle_\theta$  have equal probabilities of occupation (of 1/2) but with uncorrelated probability amplitude coefficients. Under these conditions, the radiation intensity is given by can be evaluated with

$$I(t) = \hbar\omega_0 [P_{1,0_\theta}(t) \gamma_{1,0_\theta \rightarrow 1,-1} + P_{0,0_\theta}(t) \gamma_{0,0_\theta \rightarrow 1,-1}], \quad (\text{A11})$$

where  $P_{r,m_\theta}(t)$  is the probability of being in state  $|r, m\rangle_\theta$  at time  $t$ ; the different  $P_{r,m_\theta}(t)$  are readily calculated from equations (A7)-(A8) and the initial probabilities. We thus have

$$I(t) = \frac{1}{2} \hbar\omega_0 \Gamma e^{-\Gamma t} \left\{ [1 + F(kz_0)] e^{-\Gamma F(kz_0)t} + [1 - F(kz_0)] e^{\Gamma F(kz_0)t} \right\}. \quad (\text{A12})$$

The two limits given in equations (9)-(10) result from this relation.

The transition rates for superabsorption are obtained when the two-atom system is initially in the ground  $|1, -1\rangle$  state and subjected to an incident one-photon field. It is then found that the transition rates of equations (5)-(8) are reversed [21]. That is,

$$\frac{d\gamma_{1,-1 \rightarrow 1,0_\theta}}{d\Omega} = 2 \frac{d\Gamma}{d\Omega} \quad (\text{A13})$$



$$\frac{d\gamma_{1,-1\rightarrow 0,0_\theta}}{d\Omega} = 0 \quad (\text{A14})$$

$$\frac{d\gamma_{1,0_\theta\rightarrow 1,1}}{d\Omega'} = 2 \cos^2 \left[ \frac{1}{2} k z_0 (\cos \theta' - \cos \theta) \right] \frac{d\Gamma}{d\Omega'} \quad (\text{A15})$$

$$\frac{d\gamma_{0,0_\theta\rightarrow 1,1}}{d\Omega'} = 2 \sin^2 \left[ \frac{1}{2} k z_0 (\cos \theta' - \cos \theta) \right] \frac{d\Gamma}{d\Omega'} \quad (\text{A16})$$

with  $\theta$  and  $\theta'$  denoting the orientations of the first and second absorbed photons, respectively, relative to the  $z$ -axis. Here again, there is angular correlation, but this time between successively absorbed photons.

## A.2 Energy trapping efficiency for $n$ atoms

For the two-atom problem only two permutation symmetries are available for the Dicke states: the totally symmetric species is shared by the  $r = 1$  triplet (equations 1-3), while the lone  $r = 0$  singlet is anti-symmetric (equation 4). In the more general case where the gas is composed of an arbitrary number of atoms  $n$  a larger number of symmetries, tied to the cooperative number  $r$ , exist for the Dicke states (see Fig. 1).

Although it is in principle possible to extend the spontaneous emission rates analysis for finite separations performed for the two-atom case to the  $n$ -atom problem using appropriate Dicke states, the calculations quickly become prohibitive even for a restricted number of radiators. It is, however, possible to determine the ratio of numbers of photons emitted in the small and infinite-size samples when  $m = 0$  initially, as done in equation (11) for the two-atom problem. For this, we use the known level of degeneracy of states as a function of the cooperative number  $r$  [1]

$$g_r = \frac{n! (2r + 1)}{(n/2 + r + 1)! (n/2 - r)!}, \quad (\text{A17})$$

with the fact that, for  $n$  even, the number of photons emitted from  $m = 0$  for the small and infinite-size samples are  $r$  and  $n/2$ , respectively. We thus find for the energy trapping efficiency

$$\eta = 1 - \frac{2 \sum_{r=0}^{n/2} g_r r}{n \sum_{r=0}^{n/2} g_r}. \quad (\text{A18})$$

One can readily verify that  $\eta = 1/2$  for the two-atom case, while it is 0.69 for  $n = 10$ , 0.88 for  $n = 100$ , etc. Furthermore, it is known that  $\overline{r(r+1)} \simeq m^2 + n/2$  whenever  $n \gg 1$  and  $\hbar\omega_0 \ll k_B T_{\text{kin}}$  [1], which from equation (A18) yields  $\eta \approx 1 - \sqrt{2/n}$  when  $m = 0$ .

## Appendix B The master equation

The master equation used for the analysis presented in Sec. 2.2 is as follows

$$\frac{d\hat{\rho}}{dt} = \frac{1}{i\hbar} \hbar\omega_0 \sum_j \left[ \hat{R}_j^3, \hat{\rho} \right] - \frac{\Gamma}{i} \sum_{i \neq j} \Omega_{ij} (k\Delta r_{ij}) \left[ \hat{R}_i^+ \hat{R}_j^-, \hat{\rho} \right]$$

$$-\frac{\Gamma}{2} \sum_{ij} F_{ij}(k\Delta r_{ij}) \left( \hat{R}_i^+ \hat{R}_j^- \hat{\rho} + \hat{\rho} \hat{R}_i^+ \hat{R}_j^- - 2\hat{R}_j^- \hat{\rho} \hat{R}_i^+ \right) \quad (\text{B19})$$

with

$$F_{ij}(k\Delta r_{ij}) = \frac{3}{2} \left\{ \left[ 1 - (\boldsymbol{\epsilon}_\mu \cdot \boldsymbol{\epsilon}_r)^2 \right] \frac{\sin(k\Delta r_{ij})}{k\Delta r_{ij}} + \left[ 1 - 3(\boldsymbol{\epsilon}_\mu \cdot \boldsymbol{\epsilon}_r)^2 \right] \left[ \frac{\cos(k\Delta r_{ij})}{(k\Delta r_{ij})^2} - \frac{\sin(k\Delta r_{ij})}{(k\Delta r_{ij})^3} \right] \right\} \quad (\text{B20})$$

$$\Omega_{ij}(k\Delta r_{ij}) = \frac{3}{4} \left\{ \left[ 1 - (\boldsymbol{\epsilon}_\mu \cdot \boldsymbol{\epsilon}_r)^2 \right] \frac{\cos(k\Delta r_{ij})}{k\Delta r_{ij}} - \left[ 1 - 3(\boldsymbol{\epsilon}_\mu \cdot \boldsymbol{\epsilon}_r)^2 \right] \left[ \frac{\sin(k\Delta r_{ij})}{(k\Delta r_{ij})^2} + \frac{\cos(k\Delta r_{ij})}{(k\Delta r_{ij})^3} \right] \right\} \quad (\text{B21})$$

and where  $\hat{\rho}$  is the density matrix for the atomic system,  $\Delta r_{ij} = |\mathbf{r}_i - \mathbf{r}_j|$  is the distance between atoms  $i$  and  $j$ ,  $\boldsymbol{\epsilon}_r = (\mathbf{r}_i - \mathbf{r}_j)/\Delta r_{ij}$  and  $\Gamma$  is given by equation (A10). In all calculations presented in Sec. 2.2 we set  $\boldsymbol{\epsilon}_\mu \cdot \boldsymbol{\epsilon}_r = 0$  for simplicity.

The time evolution equations for the two-atom populations presented in Figure 2 (black curves) are obtained with equations (B19)-(B21). Equilibrium conditions are imposed by adding a relaxation term acting on a time-scale  $T_1$  and a constant pump term, which we then define as  $\rho_{jj}^{\text{eq}}/T_1$ , with  $\rho_{jj}^{\text{eq}}$  the equilibrium condition for the corresponding population. We thus write

$$\frac{d\rho_{11}}{dt} = -\Gamma(1 + F_{12})\rho_{11} - \frac{(\rho_{11} - \rho_{11}^{\text{eq}})}{T_1} \quad (\text{B22})$$

$$\frac{d\rho_{22}}{dt} = -\Gamma(1 - F_{12})\rho_{22} - \frac{(\rho_{22} - \rho_{22}^{\text{eq}})}{T_1} \quad (\text{B23})$$

$$\frac{d\rho_{33}}{dt} = \Gamma(1 + F_{12})\rho_{11} + \Gamma(1 - F_{12})\rho_{22} - \frac{(\rho_{33} - \rho_{33}^{\text{eq}})}{T_1}. \quad (\text{B24})$$

The steady-state solution of these equations yields

$$\rho_{11}^{\text{ss}} = \frac{\rho_{11}^{\text{eq}}}{(1 + F_{12})\Gamma T_1 + 1} \simeq \frac{\rho_{11}^{\text{eq}}}{(1 + F_{12})\Gamma T_1} \quad (\text{B25})$$

$$\rho_{22}^{\text{ss}} = \frac{\rho_{22}^{\text{eq}}}{(1 - F_{12})\Gamma T_1 + 1} \simeq \rho_{22}^{\text{eq}} \quad (\text{B26})$$

$$\begin{aligned} \rho_{33}^{\text{ss}} &= (1 + F_{12})\Gamma T_1 \rho_{11}^{\text{ss}} + (1 - F_{12})\Gamma T_1 \rho_{22}^{\text{ss}} + \rho_{33}^{\text{eq}} \\ &\simeq \rho_{11}^{\text{eq}} + (1 - F_{12})\Gamma T_1 \rho_{22}^{\text{eq}} + \rho_{33}^{\text{eq}}, \end{aligned} \quad (\text{B27})$$

where the approximations apply whenever  $\Gamma T_1 \gg 1$  and  $F_{12}(kz_0) \simeq 1$ . Since internal energy trapping is due to non-zero steady-state values in the upper populations  $\rho_{11}$  and  $\rho_{22}$ , we find that the presence of equilibrium conditions effectively causes this trapping to take place. One also readily verifies from equations (B25)-(B26) that no

energy can be trapped when  $T_1 \rightarrow \infty$ , which is the case shown with the black curves in Figure 2.

## Appendix C The Maxwell-Bloch equations

Assuming propagation along the  $z$ -axis, the Maxwell-Bloch equations (MBE) [5, 12, 20] for a magnetic dipole transition are [6]

$$\frac{\partial n'}{\partial \tau} = \frac{i}{\hbar} (M^+ B^+ - B^- M^-) - \frac{n' - n'_{\text{eq}}}{T_1} \quad (\text{C28})$$

$$\frac{\partial M^+}{\partial \tau} = \frac{2i\mu^2}{\hbar} B^- n' - \frac{M^+}{T_2} \quad (\text{C29})$$

$$\frac{\partial B^+}{\partial z} = \frac{i\mu_0\omega_0}{2c} M^-, \quad (\text{C30})$$

where  $n' = (n_b - n_a)/2$  with  $n_a$  and  $n_b$  the densities of atoms in the lower and upper states, respectively, and  $M^+$  and  $B^+$  the amplitudes of the atomic magnetization and the magnetic induction field. The temporal derivatives are in relation to the retarded time  $\tau = t - z/c$ . The ‘‘slowly varying envelope approximation’’ is used with the magnetization and magnetic field vectors given by

$$\mathbf{M}^\pm(z, \tau) = M^\pm(z, \tau) e^{\pm i\omega_0\tau} \boldsymbol{\epsilon}_\mu \quad (\text{C31})$$

$$\mathbf{B}^\pm(z, \tau) = B^\pm(z, \tau) e^{\mp i\omega_0\tau} \boldsymbol{\epsilon}_\mu. \quad (\text{C32})$$

As for the master equation (see equations B22-B24), we added relaxation and dephasing terms with corresponding time-scales  $T_1$  and  $T_2$ , as well as enforcing equilibrium conditions through  $n'_{\text{eq}}$ . We can relate this framework to that used in Secs. 2.1 and 2.2 through the correspondences

$$n' \rightarrow \frac{1}{\delta\mathcal{V}} \sum_{j \in \delta\mathcal{V}} \hat{R}_j^3 \quad (\text{C33})$$

$$M^+ \rightarrow \frac{\mu}{\delta\mathcal{V}} \sum_{j \in \delta\mathcal{V}} \hat{R}_j^+ e^{ikz_j}, \quad (\text{C34})$$

at a given position  $z$  with  $\delta\mathcal{V}$  the volume occupied by the gas in the vicinity. In our analysis and discussion we consider  $n_- \equiv 2n' = n_b - n_a$  instead of  $n'$ . Furthermore, we are mainly concerned with conditions of thermal equilibrium or, more generally, situations where  $n_b < n_a$ . We thus have, unless otherwise indicated,  $n_- < 0$ .

As stated in Sec. 2.3, the system is subjected to an incident magnetic field  $B_0 \equiv B^+(0, \tau)$ , which effectively serves as a boundary condition at the input  $z = 0$  of the system, and internal quantum fluctuations throughout the system at  $\tau = 0$ . These fluctuations are modeled as an initial magnetization  $M^+(z, 0) = n_-^{\text{eq}} \mu \theta_0 / 2$ , where  $\theta_0 = \sqrt{2N} / |N_-^{\text{eq}}|$  is the initial ‘‘rising’’ angle [20] with  $N = N_a + N_b$  the total number of atoms ( $N_a$  and  $N_b$  in the lower and upper states, respectively) and  $N_-^{\text{eq}} = N_b^{\text{eq}} - N_a^{\text{eq}}$

(see Appendix C.1). Unlike for our discussion of Dicke's work in Sec. 2.1 and Appendix A, we express numbers of atoms using capitalized letters starting in Sec. 2.3 to avoid potential confusion with number densities.

Since phase coherence is expected for the radiation field and that this cannot take place over an arbitrarily large volume, we enforce a Fresnel number of unity and focus our analysis on a cylinder of cross-section area  $A = \lambda L$ , with  $L$  the length of the cylinder and  $\lambda$  the wavelength of radiation [20]. We then have for the relevant numbers of atoms  $N_a = n_a AL$ , etc. Our slab is therefore composed of a very large number of independent cylinders.

### C.1 Initial Bloch angle and magnetization

We require initial conditions for the integration of the MBE in equations (C28)-(C30). While  $n'_-(z, 0) = n^{\text{eq}}/2$ , it is clear from an inspection of the MBE that in the absence of an incident signal (i.e., when  $B^+(0, \tau) = 0$ ) we have  $B^+(z, \tau) = M^+(z, \tau) = 0$  if  $M^+(z, 0) = 0$ . In reality, internal quantum fluctuations modeled through the initial Bloch angle  $\theta(0)$  (see below) will cause a corresponding magnetization that will start the response from the gas. Here, we closely follow the treatment developed for superradiance by Gross and Haroche [20] but adapt it to our problem.

With  $\hat{R}^\pm = \sum_j \hat{R}_j^\pm$ , we start by noting that [35]

$$\hat{R}^\pm |r, m\rangle = \sqrt{(r \mp m)(r \pm m + 1)} |r, m \pm 1\rangle, \quad (\text{C35})$$

which in turn leads to

$$\begin{aligned} \left(\hat{R}^-\right)^p |r, m\rangle &= [(r+m) \dots (r+m-p) \\ &\times (r-m+1) \dots (r-m+p)]^{1/2} |r, m-p\rangle. \end{aligned} \quad (\text{C36})$$

and

$$\begin{aligned} \langle r, m | \left(\hat{R}^+\right)^p \left(\hat{R}^-\right)^q |r, m\rangle &= (r+m) \dots (r+m-p) \\ &\times (r-m+1) \dots (r-m+p) \delta_{pq}. \end{aligned} \quad (\text{C37})$$

At a given position  $z$  the magnetization will be defined by the atoms in the vicinity (see equation C34) and we can approximately replace  $\hat{R}^\pm$  by  $\hat{R}_k^\pm$  in equation (C37).

When  $p \ll |m| \approx r$  we have

$$\langle r, m | \left(\hat{R}_k^+\right)^p \left(\hat{R}_k^-\right)^q |r, m\rangle \simeq \delta_{pq} p! (2r)^p, \quad (\text{C38})$$

which is the situation considered by Gross and Haroche for superradiance with  $r = N/2$  [20]. On the other hand, whenever  $p \ll |m| \lesssim r$  equation (C37) reduces to

$$\langle r, m | \left(\hat{R}_k^+\right)^p \left(\hat{R}_k^-\right)^q |r, m\rangle \simeq \delta_{pq} (r^2 - m^2)^p. \quad (\text{C39})$$

At thermal equilibrium when  $|m| \ll N/2$ , calculations are complicated by the very high degeneracy of states. However, we can simplify matters by considering the mean values  $\overline{m}$  and  $\overline{r(r+1)}$ . Whenever  $\hbar\omega_0 \ll k_B T_{\text{kin}}$ , which is the case for the 21 cm line, these are found to be [1]

$$\overline{m} \simeq \frac{N}{4} \frac{\hbar\omega_0}{k_B T_{\text{kin}}} \quad (\text{C40})$$

$$\overline{r(r+1)} \simeq m^2 + \frac{N}{2}, \quad (\text{C41})$$

where the latter is valid for any  $m$  satisfying our assumption and  $k_B$  is the Boltzmann constant. With these relations we can now use equation (C39) to find

$$\langle \overline{r}, \overline{m} | \left( \hat{R}_k^+ \right)^p \left( \hat{R}_k^- \right)^q | \overline{r}, \overline{m} \rangle \simeq \delta_{pq} \left( \frac{N}{2} \right)^p. \quad (\text{C42})$$

Once again following Gross and Haroche [20], we assign the result for an initial measurement on  $\hat{R}_k^+$  to be

$$\langle \overline{r}, \overline{m} | \hat{R}_k^+ (0) | \overline{r}, \overline{m} \rangle \equiv \beta e^{i\varphi} \quad (\text{C43})$$

with  $\beta$  and  $\varphi$  random variables. We thus seek probability distributions  $P(\beta^2)$  and  $Q(\varphi)$  such that

$$\iint P(\beta^2) Q(\varphi) \beta^{2p} d(\beta^2) d\varphi = \left( \frac{N}{2} \right)^p, \quad (\text{C44})$$

with the outcome  $P(\beta^2) = \delta(\beta^2 - N/2)$ ,  $Q(\varphi) = 1/2\pi$  and  $\overline{\beta^2} = N/2$ .

Further considerations and transformations of the MBE (with  $T_1 = T_2 \rightarrow \infty$  in equations C28-C29) reveal that  $(\mu n'_-)^2 + M^+ M^-$  is a conserved quantity over time. This motivates the definition of classical versions for the pseudo-spin operators as [20]

$$R^3(\tau) = \frac{|N_-^{\text{eq}}|}{2} \cos[\theta(\tau)] \quad (\text{C45})$$

$$R_k^+(\tau) = \frac{|N_-^{\text{eq}}|}{2} \sin[\theta(\tau)] e^{i\varphi}. \quad (\text{C46})$$

Setting the initial Bloch angle to  $\theta(0) = \pi - \epsilon$ , with  $\epsilon \ll 1$ , we find from equations (C43) and (C46) that  $\epsilon = 2\beta/|N_-^{\text{eq}}|$  and

$$\begin{aligned} \theta_0 &\equiv \sqrt{\epsilon^2} \\ &= \frac{\sqrt{2N}}{|N_-^{\text{eq}}|} \end{aligned} \quad (\text{C47})$$

for the initial ‘‘rising’’ angle. From equations (C34) and (C46)-(C47), the initial magnetization becomes

$$M^+(z, 0) = \frac{1}{2}n_-^{\text{eq}}\mu\theta_0. \quad (\text{C48})$$

## C.2 Linear regime solutions

In the linear regime when  $I \ll I_{\text{sat}}$ , the magnetic field and the polarization are small and we expect  $\partial n_- / \partial \tau \approx 0$ , implying that  $n_- = n_-^{\text{eq}}$  is constant. Equations (C29)-(C30) then reduce to a simple system of linear differential equations. These equations can be solved using Laplace transforms, with the  $z \leftrightarrow u$  and  $\tau \leftrightarrow s$  correspondences, leading to

$$B_1^+(u, s) = B_0 \frac{s + 1/T_2}{us(s + 1/T_2 + 1/uLT_R)} \quad (\text{C49})$$

when the system is subjected to an incident magnetic field of amplitude  $B_0 \equiv B^+(z = 0, \tau)$  and

$$B_2^+(u, s) = i \frac{n_-^{\text{eq}}\mu_0\omega_0\mu\theta_0}{4c} \frac{1}{u^2(s + 1/T_2 + 1/uLT_R)} \quad (\text{C50})$$

when responding to initial internal magnetization fluctuations  $M^+(z, 0) = n_-^{\text{eq}}\mu\theta_0/2$ . These two solutions are uncorrelated since  $\theta_0$  is a random process.

Effecting a first inverse Laplace transform to recover the retarded time  $\tau$  and then a second to recover  $z$ , using

$$\mathcal{L}^{-1} \left\{ \frac{e^{-a/u}}{u^n} \right\} = \left( \frac{z}{a} \right)^{\frac{n-1}{2}} J_{n-1}(2\sqrt{az}), \quad (\text{C51})$$

with  $J_p(x)$  the Bessel function of the first kind and order  $p$  [36], we find

$$B_1^+(z, \tau) = B_0 \left\{ e^{-\alpha z/2} + \frac{\alpha}{2} e^{-\tau/T_2} \left[ e^{-\alpha z/2} \star J_0 \left( 2\sqrt{\frac{z\tau}{LT_R}} \right) \right] \right\} \quad (\text{C52})$$

$$B_2^+(z, \tau) = -i \frac{\hbar\theta_0}{2\mu T_R} e^{-\tau/T_2} \frac{z}{L} \sqrt{\frac{LT_R}{z\tau}} J_1 \left( 2\sqrt{\frac{z\tau}{LT_R}} \right) \quad (\text{C53})$$

with  $\alpha$  and  $T_R$  defined in equations (13)-(14). In equation (C52) ‘ $\star$ ’ stands for a spatial convolution.

The evolution time-scale of the system subjected to an incident field can be calculated as follows. As a first step, expanding the Bessel function for  $z\tau \ll LT_R$  in

equation (C52) allows us to approximate

$$B_1^+(z, \tau) \simeq B_0 \left[ e^{-\alpha z/2} \left( 1 - e^{-\tau/T_2} e^{-2\sqrt{z\tau/LT_R}} \right) + e^{-\tau/T_2} e^{-2\sqrt{z\tau/LT_R}} \right]. \quad (\text{C54})$$

If we further restrict ourselves to  $T_2 \ll T_R$ , then expanding the square root about  $zT_2/LT_R$  in equation (C54) yields

$$e^{-\tau/T_2} e^{-2\sqrt{z\tau/LT_R}} \approx e^{-\tau \left( 1 + \sqrt{zT_2/LT_R} \right) / T_2} \quad (\text{C55})$$

and an evolution time-scale given by

$$T_{\text{tr}} \approx T_2 \left( 1 + \sqrt{\frac{zT_2}{LT_R}} \right)^{-1}. \quad (\text{C56})$$

### C.3 Non-coherent radiation intensity

The non-coherent radiation intensity used for normalization in Figure 7 and the related discussion is defined with  $N_b$  atoms in the excited state [6, 7]

$$\begin{aligned} I_{\text{nc}} &= N_b \frac{\hbar\omega_0\Gamma}{A} \frac{\phi_D}{8\pi/3} \\ &= \frac{n_b}{|n_-^{\text{eq}}|} \frac{\hbar\omega_0}{AT_R}, \end{aligned} \quad (\text{C57})$$

where  $\phi_D = \lambda^2/A$  is the diffraction solid-angle at the end of our (cylindrical) system.

## Appendix D Collision cross-section

We consider a two-atom system initially in the state

$$|\psi_0\rangle = |\mathbf{P}, \Delta\mathbf{p}\rangle |bb\rangle |0\rangle, \quad (\text{D58})$$

where  $\mathbf{P} = \mathbf{p}_1 + \mathbf{p}_2$  and  $\Delta\mathbf{p} = (\mathbf{p}_2 - \mathbf{p}_1)/2$  with  $\mathbf{p}_1$  and  $\mathbf{p}_2$  the linear momenta of the first and second atoms, respectively, and the last state  $|0\rangle$  stands for the vacuum radiation field. We will assume that the two atoms are at resonance, i.e.,  $\Delta\mathbf{p} = 0$  initially. We rewrite the interaction term of the Hamiltonian in equation (A2) as follows

$$\hat{V} = -i \sum_q \frac{1}{2} \hbar\Omega_q \sum_{j=1}^2 \left[ \hat{R}_j^+ \hat{T}_q(\hbar\mathbf{k}_q) \hat{a}_q - \hat{R}_j^- \hat{T}_q^\dagger(\hbar\mathbf{k}_q) \hat{a}_q^\dagger \right] \quad (\text{D59})$$

with  $\hat{T}_q(\hbar\mathbf{k}_q) = e^{i\mathbf{k}_q \cdot \hat{\mathbf{r}}}$  the linear momentum translation operator [37].

Using a first-order perturbation expansion, it can be shown that the state of the system after the emission of a first photon is composed of a superposition of states of the form

$$|\psi_+\rangle = \frac{1}{\sqrt{2}} (|\hbar\mathbf{k}_r/2\rangle |ab\rangle + |-\hbar\mathbf{k}_r/2\rangle |ba\rangle) |\mathbf{P} - \hbar\mathbf{k}_r\rangle |1_r\rangle \quad (\text{D60})$$

that differ only in the radiation mode of the emitted photon. In equation (D60) the radiation state  $|1_r\rangle$  implies that one photon occupies mode  $r$  and all other modes are empty. After a short time the photon leaves the system and  $|1_r\rangle$  is replaced by  $|0\rangle$ .

We can express this state using the position basis  $|\mathbf{R}, \Delta\mathbf{r}\rangle$ , where  $\mathbf{R} = (\mathbf{r}_1 + \mathbf{r}_2)/2$  and  $\Delta\mathbf{r} = \mathbf{r}_2 - \mathbf{r}_1$  are conjugate to  $\mathbf{P}$  and  $\Delta\mathbf{p}$ , respectively, to get

$$\begin{aligned} |\psi_+\rangle &\propto \int d^3R e^{i(\mathbf{P}/\hbar - \mathbf{k}_r) \cdot \mathbf{R}} |\mathbf{R}\rangle \int d^3\Delta\mathbf{r} |\Delta\mathbf{r}\rangle \\ &\times \frac{1}{\sqrt{2}} \left( e^{i\mathbf{k}_r \cdot \Delta\mathbf{r}/2} |ab\rangle + e^{-i\mathbf{k}_r \cdot \Delta\mathbf{r}/2} |ba\rangle \right) |0\rangle. \end{aligned} \quad (\text{D61})$$

We recognize on the last line the internal state  $|1, 0\rangle_\theta$  of equation (2) when  $\mathbf{k}_r$  makes an angle  $\theta$  with  $\Delta\mathbf{r}$ . The state orthogonal to  $|\psi_+\rangle$ , and related to  $|0, 0\rangle_\theta$  in equation (4), is

$$\begin{aligned} |\psi_-\rangle &\propto \int d^3R e^{i(\mathbf{P}/\hbar - \mathbf{k}_r) \cdot \mathbf{R}} |\mathbf{R}\rangle \int d^3\Delta\mathbf{r} |\Delta\mathbf{r}\rangle \\ &\times \frac{1}{\sqrt{2}} \left( e^{i\mathbf{k}_r \cdot \Delta\mathbf{r}/2} |ab\rangle - e^{-i\mathbf{k}_r \cdot \Delta\mathbf{r}/2} |ba\rangle \right) |0\rangle. \end{aligned} \quad (\text{D62})$$

As discussed in Sec. 2.3.2, after the transient regime, when the gas has become dark, every system is in a dark state such as the one given in equation (D62). Let us then consider two such systems  $A$  and  $B$  entering into a collision. We choose a reference frame at rest with the center-of-mass for the two systems such that  $\mathbf{R}_A = -\mathbf{R}_B = -\mathbf{R}_0$ . For the 21 cm line of the hydrogen atom we can assume that  $|\mathbf{P}_A|, |\mathbf{P}_B| \gg \hbar k_r$  irrespective of the radiation mode. To lighten the notation we omit the spatial states  $|\mathbf{R}_A\rangle, |\Delta\mathbf{r}_A\rangle$ , etc., and the vacuum  $|0\rangle$  state to focus on the internal states, such that we can write for the colliding system

$$\begin{aligned} |\Psi\rangle &= |\psi_-\rangle_A |\psi_-\rangle_B \\ &\propto e^{i(\mathbf{P}_B - \mathbf{P}_A) \cdot \mathbf{R}_0/\hbar} (|ab\rangle_A - |ba\rangle_A) (|ab\rangle_B - |ba\rangle_B) \\ &\propto e^{i(\mathbf{P}_B - \mathbf{P}_A) \cdot \mathbf{R}_0/\hbar} (|ab\rangle_A |ab\rangle_B + |ba\rangle_A |ba\rangle_B \\ &\quad - |ab\rangle_A |ba\rangle_B - |ba\rangle_A |ab\rangle_B). \end{aligned} \quad (\text{D63})$$

If two atoms enter into an elastic collision, say the first atoms of both pairs, then under the Born approximation each term will bring a scattering amplitude of the type



[38]

$$f(\mathbf{k}_{\text{in}}, \mathbf{k}_{\text{out}}) = -\frac{m_r}{2\pi\hbar^2} \int d^3r' e^{-i\mathbf{k}_{\text{out}}\cdot\mathbf{r}'} V(\mathbf{r}') e^{i\mathbf{k}_{\text{in}}\cdot\mathbf{r}'} \quad (\text{D64})$$

with  $\mathbf{k}_{\text{in}} = (\mathbf{P}_B - \mathbf{P}_A)/\hbar$ ,  $\mathbf{k}_{\text{out}}$  the scattered wave vector and  $m_r$  the reduced mass. For high relative speed between the colliding atoms, i.e., when  $|\mathbf{P}_B - \mathbf{P}_A|^2/2m_r \gg \hbar\omega_0$ , it is expected that the scattering amplitude will be independent of their internal states. It therefore follows from equation (D63) that under these circumstances the collision cross-section  $\sigma(\mathbf{k}_{\text{in}}, \mathbf{k}_{\text{out}}) = 0$  since it consists of the square of the sum of the four corresponding scattering amplitudes.

Although such calculations need to be generalized, we find that at high relative speed two darkened entangled systems are likely to pass through each other, unimpeded, during a collision. They would not feel the presence of each other even though individual atoms may actually collide. This is due to the destructive interference resulting from the entanglement within each of the systems.

Finally, it is interesting to note that in cases where the states are totally symmetric the cross-section scales as  $N^2\sigma_0$ , where  $N$  is the number of atoms and  $\sigma_0$  the one-atom cross-section.